Editors' Suggestion

Combined surface x-ray diffraction and density functional theory study of the germanene/Al(111)-($\sqrt{7} \times \sqrt{7}$)*R*19.1° structure

K. Zhang,[1] M.-C. Hanf,[3,4] D. Sciacca,[2] R. Bernard,[1] Y. Borensztein,[1] A. Resta,[5] Y. Garreau,[5,6] A. Vlad,[5] A. Coati,[5] I. Lefebvre,[2] M. Derivaz,[3,4] C. Pirri,[3,4] P. Sonnet,[3,4] R. Stephan,[3,4] and G. Prévot[1,*]

[1]*Sorbonne Université, Centre National de la Recherche Scientifique, Institut des NanoSciences de Paris, INSP, F-75005 Paris, France*
[2]*Université de Lille, CNRS, Centrale Lille, Université Polytechnique Hauts-de-France, Junia-ISEN, UMR 8520 - IEMN, F-59000 Lille, France*
[3]*Université de Haute Alsace, CNRS, IS2M UMR7361, F-68100 Mulhouse, France*
[4]*Université de Strasbourg, 67000 Strasbourg, France*
[5]*Synchrotron SOLEIL, L'Orme des Merisiers Saint-Aubin, Boîte Postale 48, 91192 Gif-sur-Yvette Cedex, France*
[6]*Université Paris Cité, Laboratoire Matériaux et Phénomènes Quantiques, CNRS, F-75013, Paris, France*

(Received 11 April 2022; revised 19 June 2022; accepted 21 June 2022; published 12 July 2022)

Several studies have reported the possible growth of germanene on various metal surfaces. However, the exact structure of the layers formed upon evaporation at or above room temperature remains controversial. In particular, the layers obtained after Ge deposition on Al(111) have been either considered as honeycomb organization of Ge atoms on top of a nonreconstructed substrate, or as alloyed layers. Using quantitative measurements by surface x-ray diffraction compared to density functional theory calculations, we show that the ($\sqrt{7} \times \sqrt{7}$)$R \pm 19.1°$ reconstruction obtained after room temperature deposition is a mixed Ge-Al honeycomb layer, on top of an Al(111) plane, and not a pure germanene layer.

DOI: 10.1103/PhysRevB.106.045412

I. INTRODUCTION

As graphene analogs, honeycomb monolayers of other group 14 elements (Si, Ge, Sn, Pb) have attracted a great interest for electronic applications. Intensive efforts to synthesize silicene, germanene, stanene, and plumbene have been made after the prediction of a metastable state for freestanding silicene and germanene [1,2]. Up to now, a large consensus has been established concerning the effective synthesis of silicene on Ag(111) and (110) substrates [3,4], and convincing results have been obtained for the growth of stanene on Cu(111) [5] and plumbene on Fe/Ir(111) [6]. For these last two cases, it is worth noting that the monolayers have been obtained by depositing Sn or Pb atoms at low temperature, respectively, at 200 and 140 K. On the contrary, it has been shown that for deposition at or above room temperature, deposited atoms could easily form surface alloys [7,8]. For growth of silicene on Ag(111), exchange between Si and Ag atoms has also been observed under such experimental conditions but this leads to the formation of silicene domains inserted in the Ag(111) surface plane [9,10]. As concerns the possible formation of germanene, contradictory works have been reported. Germanene synthesis on metal substrates was first reported in 2014 on Pt(111) [11], and then on GePt/Ge(110) [12], Au(111) [13], Al(111) [14], Cu(111) [15], or Ag(111) [16]. For all these cases, either Ge was evaporated onto a substrate held above room temperature, typically in the 360–473 K temperature range [13,14,16], or onto a substrate maintained at room temperature and further annealed in the 450–1100 K temperature range [11,12,15]. The possible germanene formation was then derived from scanning tunneling microscopy (STM) measurements and density functional theory (DFT) computations. However, alloy formation has been suggested in the case of Ge/Pt(111) [17], Ge/Ag(111) [18], Ge/Au(111) [19], and Ge/Al(111) growth [20], at or above room temperature, raising doubts concerning the possible germanene formation on these substrates. Note that such controversy exists also for other elemental monolayers such as borophene [21,22].

In order to determine the exact structure and composition of Ge/Ag(111) and Ge/Al(111) layers previously assigned to germanene, we have recently combined surface x-ray diffraction (SXRD) measurements and DFT simulations [23,24]. For Ge/Ag(111), we have shown that the structure formed after deposition at 420 K and assigned previously to a striped honeycomb pattern [16] was in fact an Ag_2Ge surface alloy, confirming STM observations of the growth dynamics [25]. For Ge/Al(111), we have studied the structure obtained after deposition at 373K, showing a (3×3) reconstruction with respect to the Al(111) substrate [14]. It was initially proposed to correspond to a (2×2) reconstruction of a germanene honeycomb layer, i.e., with eight Ge atoms per unit cell [14]. Recent high resolution STM observations have also evidenced the presence, at the surface, of eight atoms per unit cell [24]. However, it was also suggested from DFT calculations that this structure could correspond to a surface alloy [26], in agreement with low energy electron diffraction and ion scattering measurements [20]. Very recently, our SXRD results unambiguously showed that the (3×3) reconstruction is related to a two-layer surface alloy, i.e., a mixed Al-Ge honeycomb layer on top of a substitutional Al-Ge alloy, with the

*prevot@insp.jussieu.fr

possible following composition: Ge_4Al_4/Ge_2Al_7 [24]. From these two studies, we can conclude that for growth at a substrate temperature around 373 K, formation of a surface alloy occurs at the expense of a pure germanium monolayer.

As stanene or plumbene growth is observed for low temperature deposition, whereas alloying occurs for deposition above room temperature, one may wonder if lowering the substrate temperature during Ge/Al(111) deposition could, in a similar way, promote the formation of germanene. Indeed, it has been observed that growth of Ge on Al(111) at room temperature leads to the formation of another structure, corresponding to a $(\sqrt{7} \times \sqrt{7})R \pm 19.1^\circ$ reconstruction with respect to the substrate [27,28]. A model of $(\sqrt{3} \times \sqrt{3})$ germanene on Al$(\sqrt{7} \times \sqrt{7})$ has been proposed, associated with six Ge atoms per unit cell [28]. For this case also, good agreement is found with high resolution STM observations that show six protrusions per unit cell [29]. However, STM does not allow for a chemical characterization of the surface and the layers underneath, and some of the protrusions could correspond to Al atoms. Moreover, Ge atoms could also be inserted in the plane below the surface, as observed for the (3×3) reconstruction. In order to determine the atomic structure and the composition of the $(\sqrt{7} \times \sqrt{7})R \pm 19.1^\circ$ Ge/Al(111) reconstruction, we have thus undertaken SXRD measurements and an energetic DFT study. We demonstrate that it corresponds to a Ge-Al alloy layer on a pure Al surface.

II. METHODS

SXRD experiments were performed at the SIXS beamline of the SOLEIL synchrotron. The Al(111) sample was prepared by repeated cycles of Ar+ sputtering and annealing at $T = 750$ K. Ge was evaporated in the diffraction chamber from a crucible using a commercial Omicron Nanotechnology *e*-beam evaporator with a sample kept at 300 K. The Ge flux was kept constant during evaporation with a deposition rate of ∼1.2 ML/h, where 1 ML (monolayer) corresponds to the completion of the $(\sqrt{7} \times \sqrt{7})R \pm 19.1^\circ$ structures. The sample was analyzed with 18.46 keV x rays at a grazing incidence angle of 0.2 °. Diffracted x rays were detected by a hybrid pixel detector [30]. The diffracted intensity was measured by performing a series of rocking scans along the crystal truncation rods. A reference scan was taken periodically to correct the intensity from the variations due to the layer degradation, which was fitted with a linear decay with time constant $\tau = 0.05$ h. We used the BINOCULARS software to produce three-dimensional intensity data in the reciprocal space from the raw data [31]. The intensity was further integrated along the direction parallel to the surface to get the structure factors. For this purpose, the data were fitted with the product of a Lorentzian line shape in one direction with a Gaussian line shape in the other direction. Such line shapes were found to very well reproduce the lateral shape of the diffraction rods. We finally obtained a set of 326 structure factors along nine inequivalent reconstruction rods.

The Vienna *ab initio* simulation package (VASP) code has been used to carry out the DFT calculations [32–35], in the generalized gradient approximation (GGA), using the projector augmented plane-wave (PAW) method [36,37] and the Perdew, Burke, and Ernzerhof (PBE) exchange-correlation functional [38,39]. The Brillouin zone is described with $(5 \times 5 \times 1)$ k points. Calculations have been performed with a cutoff energy value of 450 eV, and the entire system was fully relaxed until the forces acting on each atom were less than 0.05 eV nm^{-1} . Van der Waals interactions were not taken into account since they do not affect the relative energies of the different tested models. Band structure calculations have been performed using the BANDUP code [40,41]. Local density of states (LDOS) images are obtained using Tersoff-Hamann approximation [42]. The unit cell corresponds to a $(\sqrt{7} \times \sqrt{7})$ Al(111) surface mesh, with a PBE DFT optimized lattice parameter of 0.7558 nm [43]. The tested models correspond to the best models obtained from the SXRD initial fitting procedure. The slab is made of ten planes, each of them containing seven Al atoms, corresponding to bulk aluminum, and one surface layer of six atoms arranged in a honeycomb lattice, which are Ge atoms only, or a mixing of Ge and Al atoms. Only the bottom Al plane was kept fixed during relaxation (similar to the procedure adopted in Refs. [24,44]). The vacuum region is 9 Å thick. The atomic structures are presented using the VISUAL MOLECULAR DYNAMIC software developed by the Theoretical and Computational Biophysics Group in the Beckman Institute for Advanced Science and Technology at the University of Illinois at Urbana-Champaign [45,46].

III. RESULTS

In the following, the (H, K, L) indices used for indexing a reflection in reciprocal space refer to the Al(111) $(\sqrt{7} \times \sqrt{7})$ reconstruction basis ($a = 0.7577$ nm, $b = 0.7577$ nm, $c = 0.7014$ nm, $\alpha = \beta = 90^\circ$, $\gamma = 120^\circ$), while (h, k, l) indices correspond to the Al(111) surface unit cell. During Ge deposition on the Al substrate held at 300 K, we have followed by SXRD the evolution of the intensity for the $(H, K, L) = (1, 1, 0.1)$ reflection. As soon as evaporation starts, a diffraction peak appears, indicating that $(\sqrt{7} \times \sqrt{7})$ reconstructed domains have formed on the surface. The evaporation was stopped at intensity saturation of this peak. After evaporation, the full width at half maximum (FWHM) of the peak at $(H, K, L) = (1, 1, 0.1)$ is $\Delta q = 0.08$ nm^{-1} . This corresponds to a mean domain size of around $2\pi/\Delta q = 80$ nm. In order to check the possible presence of the (3×3) reconstruction, we have acquired a wide angular scan around the $(h, k, l) = (0, 2/3, 0.1)$ position, shown in Fig. 1. Two intense peaks are clearly visible, associated with the two domains of the $(\sqrt{7} \times \sqrt{7})R \pm 19.1^\circ$ reconstruction. On the contrary, only a small signal is found, at 0°, for the (3×3) reconstruction, whereas we had previously measured a high intensity for this reflection, for a deposition temperature of 373 K [24]. This indicates that, for Ge growth at room temperature, the surface is mostly covered with the $(\sqrt{7} \times \sqrt{7})R \pm 19.1^\circ$ reconstruction and that the coverage of (3×3) domains is negligible.

In order to determine the precise atomic structure of the reconstruction, we have tested several models based on the STM observations of Muzychenko *et al.* [29,47]. We have thus assumed that the first plane contains six atoms, organized in a honeycomb pattern. This corresponds indeed to the pattern observed on extrahigh resolution STM images [29]. However, contrary to the conclusion of Muzychenko *et al.*,

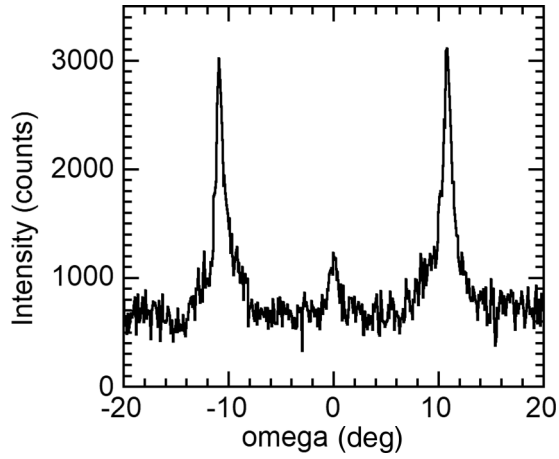

FIG. 1. Angular scan around the $(h, k, l) = (0, 2/3, 0.1)$ position. The signal corresponds to the intensity integrated for a window $0.164\ \text{nm}^{-1} < q_{//} < 0.173\ \text{nm}^{-1}$ and $0 < q_z < 0.027\ \text{nm}^{-1}$.

we have considered that some of these atoms could be Al atoms instead of Ge atoms, up to a composition of Ge_2Al_4. This assumption is justified by the fact that, in the case of the (3×3) reconstruction, we have previously shown that the surface plane is a mixed Al-Ge plane [24]. For the interface layer, we have either assumed that it is a pure Al layer, corresponding to an Al(111) plane, or to a substitutional alloy, i.e., a (111) plane where one to three Al atoms could be replaced with Ge atoms. We have assumed an overall $p3$ symmetry. For this 2D space group, atoms occupy $1a$ at $(0, 0)$, $1b$ at $(\frac{1}{3}, \frac{2}{3})$, $1c$ at $(\frac{2}{3}, \frac{1}{3})$, or $3d$ Wyckoff positions in the unit cell at (x, y), $(-y, x-y)$, $(y-x, -x)$. For the surface plane, for symmetry reasons, three atoms occupy $1a$, $1b$, and $1c$ sites and three others are in $3d$ equivalent sites. This leads to the two possible configurations for the orientation of the honeycomb, shown in Figs. 2(b) and 2(e), for the respectively written as type I and type II. For the other planes, one atom occupies a $1a$, $1b$, or $1c$ site, whereas the others are on $3d$ sites. We have thus obtained a set of 96 configurations. For each configuration, the best fit of the structure factors has been obtained by exploring the space of free parameters (an overall scale factor, the atomic positions of the first two layers and Debye-Waller parameters) using the genetic algorithm implemented in SCIPY [48]. The agreement was obtained by minimizing $(N_{\text{pts}} - N_{\text{par}})\chi^2 + E$, where E is a dimensionless Lennard-Jones interaction energy between nearest-neighbor atoms [24] which ensures that unphysical configurations, for example, exhibiting too short nearest-neighbor distances, are excluded, and where $\chi^2 = \frac{1}{N_{\text{pts}} - N_{\text{par}}} \sum_{N_{\text{Pts}}} \left(\frac{F_{\text{th}} - F_{\text{exp}}}{\sigma_{\text{exp}}}\right)^2$. $N_{\text{pts}} = 326$ is the number of experimental structure factors, $N_{\text{par}} = 27$ is the number of free parameters, and σ_{exp} is the experimental uncertainty, which takes into account the statistical uncertainty given by the number of counted photons and an overall 10% uncertainty. In order to focus on a correct reproduction of the structure factors, we have assigned a low weight to the Lennard-Jones energy. After relaxation, two configurations were found to give very good agreement with the experimental structure factors. They both correspond to a Ge_3Al_3 surface alloy on a pure Al plane. The best fit with $\chi^2 = 2.4$ corresponds to type I, whereas the other $(\chi^2 = 2.7)$ corresponds to type II. Note that these fits could have been improved by letting more Al planes below the surface be free to relax, but this would have largely increased the number of free parameters.

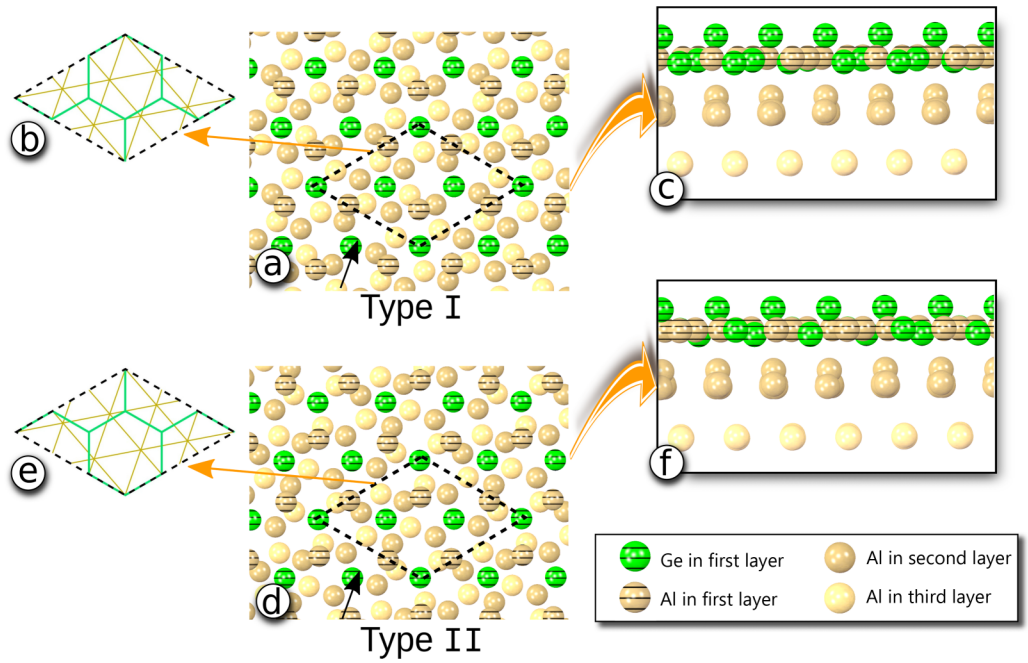

FIG. 2. Models of Ge layers on Al(111) relaxed by DFT. (a–c) type-I Ge_3Al_3/Al_7. (d–f) type-II Ge_3Al_3/Al_7. (a,d) are top views whereas (c,f) correspond to side views taken from the orientation given by the black arrows. (b,e) show the superimposition of the Al and honeycomb lattices inside the unit cell.

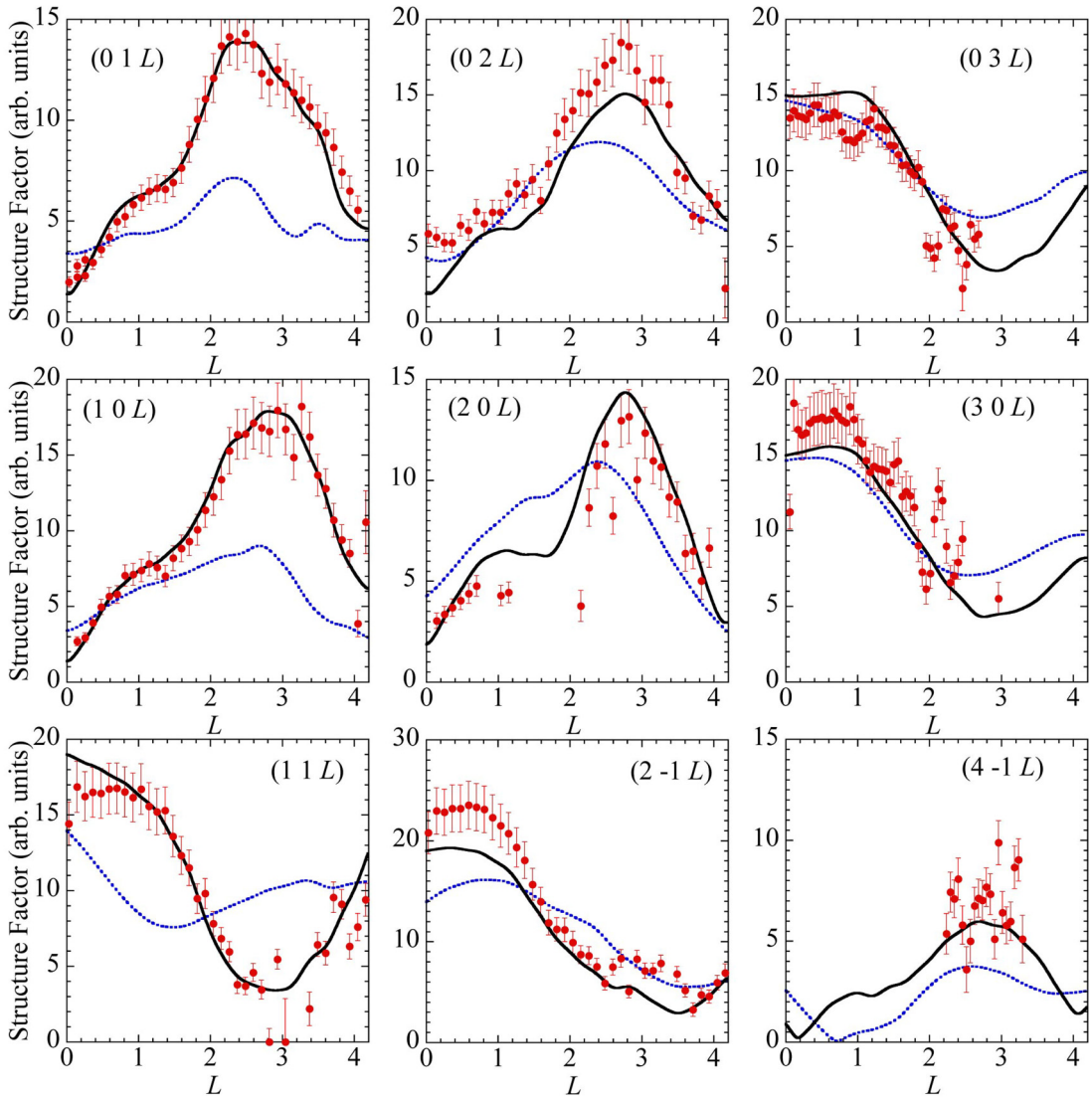

FIG. 3. Comparison between experimental (red dots) and simulated structure factors for the Ge_3Al_3/Al_7 type-I (continuous black line) and Ge_6/Al_7 type-I models (blue dotted lines), along the different measured rods.

These two configurations also correspond to low values of the Lennard-Jones energy, indicating that the interatomic distances are close to the expected ones. However, in order to obtain accurate values of the equilibrium atomic positions, these models were further relaxed by DFT calculations up to configurations of local minimum energy. The relaxed models were then used to compute again the structure factors, which were also compared with the experimental ones. The type-I model relaxes into a configuration close to the starting configuration, and corresponds to $\chi^2 = 3.4$ whereas the type-II model relaxes into slightly different positions and corresponds to $\chi^2 = 7.6$. These two relaxed configurations are shown in Fig. 2. All atoms of the surface are nearly in the same plane, except the Ge atom at the node of the unit cell, which is located 1 Å above the other surface atoms. This atom is on top of an Al atom which is also above the average height of the other Al atoms of the interface layer.

We have also compared the experimental structure factors to those obtained for a model of a pure Ge honeycomb layer on a nonreconstructed substrate. This model of a germanene layer has been initially proposed by Endo *et al.* [28], and corresponds to type-I Ge_6/Al_7. We have thus relaxed this configuration by DFT. As expected from our previous exploration of possible models, the obtained fit is poor, with $\chi^2 = 11.4$. Figure 3 shows the comparison between the experimental and simulated structure factors for the Ge_3Al_3/Al_7 and Ge_6/Al_7 models. As expected from the value of χ^2, the agreement is very good for the mixed honeycomb surface layer and poor on nearly all rods for the pure germanene layer.

We have also compared the thermodynamic stability of the different models of the $(\sqrt{7} \times \sqrt{7})R \pm 19.1^\circ$ reconstruction with the different models of the (3×3) Ge/Al(111) reconstruction that we have previously computed [24]. Since the systems differ not only by their structure but also their chemical composition, it is not easy to simply compare their total energies. Two quantities can be used: the adsorption energy per Ge atom, E_{ad}, with respect to the bulk Ge energy $E_{Ge\ bulk}$:

$$E_{ad} = (E_{Ge-Al} - E_{Al} - N_{Ge}E_{Ge\ bulk} - \Delta N_{Al}\, E_{Al\ bulk})/N_{Ge},$$

TABLE I. Adsorption energy per Ge atom computed for different models. Values for the (3 × 3) models are taken from [24].

Surface layer	Interface layer	E_{ad} (eV/at)	Unit cell
Ge_3Al_3 type-I	Al_7	–0.087	$(\sqrt{7}\times\sqrt{7})R\pm 19.1^\circ$
Ge_3Al_3 type II	Al_7	–0.058	
Ge_6 type I	Al_7	0.056	
Ge_6 type II	Al_7	0.078	
Ge_8	Al_9	0.066	(3 × 3)
Ge_4Al_4	Al_9	–0.043	
Ge_4Al_4	Ge_1Al_8	–0.031	
Ge_4Al_4	Ge_2Al_7	–0.027	
Ge_5Al_3	Al_9	–0.051	
Ge_5Al_3	Ge_1Al_8	–0.040	
Ge_5Al_3	Ge_2Al_7	–0.011	

and the formation energy per unit area, γ, which is calculated in the following way:

$$\gamma = (E_{\mathrm{Ge-Al}} - E_{\text{back side Al}} - N_{\mathrm{Ge}}\mu_{\mathrm{Ge}} - N_{\mathrm{Al}}E_{\text{Al bulk}})/A,$$

where A is the area of the $(\sqrt{7}\times\sqrt{7})R\pm 19.1^\circ$ or (3 × 3) mesh, $E_{\mathrm{Ge-Al}}$ is the total energy of the considered model, $E_{\text{back side Al}}/A$ is the surface energy of the back side of the slab, N_{Al} and N_{Ge} the number of Al and Ge atoms in the slab, μ_{Ge} the chemical potential of Ge, and E_{Al} is the energy of a slab of the same lateral size without Ge, while ΔN_{Al} is the difference of the number of Al atoms between the considered Ge/Al model and the bare Al slab. $E_{\text{Al bulk}}$ and $E_{\text{Ge bulk}}$ correspond to the energy of one Al or Ge atom within an aluminum or germanium crystal, respectively.

The adsorption energies for Ge atoms in the different models are shown in Table I. Among the models corresponding to the $(\sqrt{7}\times\sqrt{7})R\pm 19.1^\circ$ reconstruction, the type-I Ge_3Al_3/Al_7 structure possesses the lowest adsorption energy, of –0.087 eV/at. The adsorption energy for the type-II Ge_3Al_3/Al_7 structure is slightly higher (–0.058 eV/at), indicating a less stable configuration. This corroborates the results of the comparison with experimental structure factors, which indicates that the agreement with the experiments was poorer for this model. Similarly, pure germanene layers, which could not fit the x-ray experiments, correspond also to less stable configurations, with positive adsorption energies. Thus, for the $(\sqrt{7}\times\sqrt{7})R\pm 19.1^\circ$ reconstruction, alloying in the surface plane is favored with respect to pure germanene formation. Similar findings were also previously observed for the (3 × 3) reconstruction, as reported in Table I.

Figure 4 shows the evolution of the formation energy for different models as a function of $\Delta\mu_{\mathrm{Ge}}$, the deviation of μ_{Ge} with respect to $E_{\text{Ge bulk}}$. As expected from the values of Table I, the lowest curve for $\Delta\mu_{\mathrm{Ge}} = 0$ corresponds to Ge_3Al_3 type I. As the chemical potential increases, alloyed (3 × 3) models become favored. Pure germanene layers are never favored.

Finally, we have computed the theoretical STM image corresponding to the Ge_3Al_3/Al_7 model. It is shown in Fig. S1 in the Supplemental Material [49] for a negative sample bias. It is in good agreement with the corresponding experimental high resolution STM images of Muzychenko *et al.* [29]. We have also computed the theoretical band structure of a freestanding Ge_3Al_3 layer with the atomic positions identical to those of the Ge_3Al_3 type-I layer on the Al substrate. It is shown in Fig. S2 [49] and displays a metallic character.

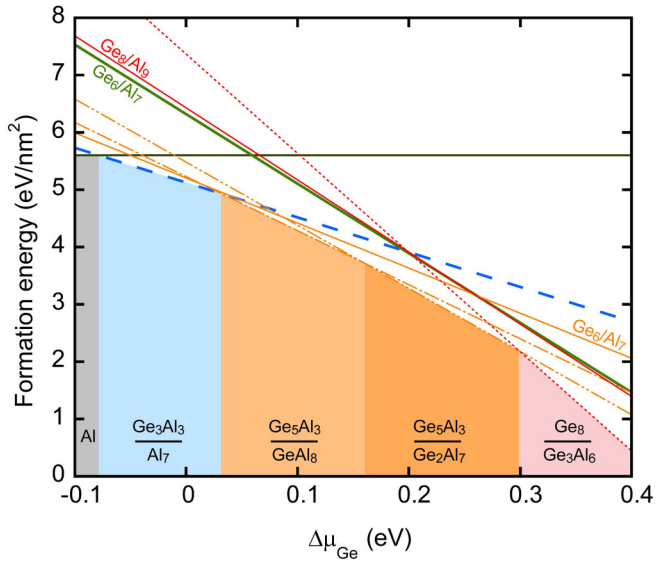

FIG. 4. Variation of the formation energy with respect to $\Delta\mu_{\mathrm{Ge}} = \mu_{\mathrm{Ge}} - E_{\text{Ge bulk}}$ for different Ge/Al(111) models. Black horizontal line: Al(111) surface. Wide lines correspond to $(\sqrt{7}\times\sqrt{7})R\pm 19.1^\circ$ models (blue dashed line: Ge_3Al_3/Al_7; green solid line: Ge_6/Al_7) whereas narrow lines correspond to (3 × 3) models (orange solid line: Ge_5Al_3/Al_9; orange dash-dot line: $Ge_5Al_3/GeAl_8$; orange dash-dot-dot line: Ge_5Al_3/Ge_2Al_7; red dotted line: Ge_8/Ge_3Al_6; red solid line: Ge_8/Al_9.

IV. CONCLUSION

We obtain remarkable agreement between SXRD and DFT results for the $(\sqrt{7}\times\sqrt{7})R\pm 19.1^\circ$ Ge/Al(111) reconstruction formed by deposition at 300 K. The best fit of the structure factors is obtained for a mixed honeycomb structure with three Ge atoms and three Al atoms in the surface plane (type-I Ge_3Al_3/Al_7). This is also, in a large range of chemical potential, the most thermodynamically stable model among those studied. It is interesting to compare these findings with the ones obtained for the (3 × 3) Ge/Al(111) reconstruction. For this reconstruction, observed for higher temperature deposition (373 K), the best fit corresponds to a two-layer surface alloy. It is thus possible that low temperature deposition hinders the formation of an alloy extending over several atomic planes. However, it has been observed that the $(\sqrt{7}\times\sqrt{7})R\pm 19.1^\circ$ Ge/Al(111) structure could also form in the 373–413 K temperature range, in the very first stage of growth [20,47]. We thus conclude that for the very first stage of growth above room temperature, the Ge chemical potential is small and growth of the $(\sqrt{7}\times\sqrt{7})R\pm 19.1^\circ$ reconstruction is favored. As Ge coverage increases, the chemical potential increases and the (3 × 3) reconstruction preferentially forms. When the growth temperature is reduced, nucleation of (3 × 3) domains, which corresponds to a two-layer thick alloy, is kinetically reduced, and only occurs at the vicinity of step edges [47]. This explains why SXRD measurements show that for

one monolayer coverage, the surface is mostly covered with $(\sqrt{7} \times \sqrt{7})R \pm 19.1^\circ$ domains for room temperature deposition, whereas it is covered with (3×3) domains after growth at 373 K.

ACKNOWLEDGMENTS

This study is financially supported the French National Research Agency (Germanene Project No. ANR-17-CE09-0021-03). K.Z. is supported by the Chinese Scholarship Council (CSC Contract No. 201808070070). The authors would like to acknowledge the High Performance Computing Center of the University of Strasbourg for supporting this work by providing scientific support and access to computing resources. Part of the computing resources were funded by the Equipex Equip@Meso project (Programme Investissements d'Avenir) and the CPER Alsacalcul/Big Data.

[1] K. Takeda and K. Shiraishi, Theoretical possibility of stage corrugation in Si and Ge analogs of graphite, Phys. Rev. B **50**, 14916 (1994).

[2] S. Cahangirov, M. Topsakal, E. Aktürk, H. Şahin, and S. Ciraci, Two- and One-Dimensional Honeycomb Structures of Silicon and Germanium, Phys. Rev. Lett. **102**, 236804 (2009).

[3] P. Vogt, P. De Padova, C. Quaresima, J. Avila, E. Frantzeskakis, M. C. Asensio, A. Resta, B. Ealet, and G. Le Lay, Silicene: Compelling Experimental Evidence for Graphenelike Two-Dimensional Silicon, Phys. Rev. Lett. **108**, 155501 (2012).

[4] T. Leoni *et al.*, Demonstration of the existence of dumbbell silicene: A stable two-dimensional allotrope of silicon, J. Phys. Chem. C **125**, 17906 (2021).

[5] J. Deng *et al.*, Epitaxial growth of ultraflat stanene with topological band inversion, Nat. Mater. **17**, 1081 (2018).

[6] G. Bihlmayer, J. Sassmannshausen, A. Kubetzka, S. Blügel, K. von Bergmann, and R. Wiesendanger, Plumbene on a Magnetic Substrate: A Combined Scanning Tunneling Microscopy and Density Functional Theory Study, Phys. Rev. Lett. **124**, 126401 (2020).

[7] J. Yuhara, Y. Fujii, K. Nishino, N. Isobe, M. Nakatake, L. Xian, A. Rubio, and G. Le Lay, Large area planar stanene epitaxially grown on Ag(1 1 1), 2D Mater. **5**, 025002 (2018).

[8] J. Yuhara, B. He, N. Matsunami, M. Nakatake, and G. Le Lay, Graphene's latest cousin: Plumbene epitaxial growth on a "nano watercube", Adv. Mater. **31**, 1901017 (2019).

[9] G. Prévot, R. Bernard, H. Cruguel, and Y. Borensztein, Monitoring Si growth on Ag(111) with scanning tunneling microscopy reveals that silicene structure involves silver atoms, Appl. Phys. Lett. **105**, 213106 (2014).

[10] R. Bernard, Y. Borensztein, H. Cruguel, M. Lazzeri, and G. Prevot, Growth mechanism of silicene on Ag(111) determined by scanning tunneling microscopy measurements and *ab initio* calculations, Phys. Rev. B **92**, 045415 (2015).

[11] L. Li, S. Lu, J. Pan, Z. Qin, Y. Wang, Y. Wang, G. Cao, S. Du, and H.-J. Gao, Buckled germanene formation on Pt(111), Adv. Mater. **26**, 4820 (2014).

[12] P. Bampoulis, L. Zhang, A. Safaei, R. van Gastel, B. Poelsema, and H. J. W. Zandvliet, Germanene termination of Ge_2Pt crystals on Ge(110), J. Phys.: Condens. Matter **26**, 442001 (2014).

[13] M. E. Dávila, L. Xian, S. Cahangirov, A. Rubio, and G. Le Lay, Germanene: A novel two-dimensional germanium allotrope akin to graphene and silicene, New J. Phys. **16**, 095002 (2014).

[14] M. Derivaz, D. Dentel, R. Stephan, M.-C. Hanf, A. Mehdaoui, P. Sonnet, and C. Pirri, Continuous germanene layer on Al(111), Nano Lett. **15**, 2510 (2015).

[15] Z. Qin, J. Pan, S. Lu, Y. Shao, Y. Wang, S. Du, H.-J. Gao, and G. Cao, Direct evidence of Dirac signature in bilayer germanene islands on Cu(111), Adv. Mater. **29**, 1606046 (2017).

[16] C.-H. Lin, A. Huang, W. W. Pai, W.-C. Chen, T.-Y. Chen, T.-R. Chang, R. Yukawa, C.-M. Cheng, C.-Y. Mou, I. Matsuda *et al.*, Single-layer dual germanene phases on Ag(111), Phys. Rev. Materials **2**, 024003 (2018).

[17] C.-S. Ho, S. Banerjee, M. Batzill, D. E. Beck, and B. E. Koel, Formation and structure of a $(\sqrt{19}\times\sqrt{19})R23.4^\circ$-Ge/Pt(111) surface alloy, Surf. Sci. **603**, 1161 (2009).

[18] H. Oughaddou, S. Sawaya, J. Goniakowski, B. Aufray, G. Le Lay, J. M. Gay, G. Tréglia, J. P. Bibérian, N. Barrett, C. Guillot *et al.*, Ge/Ag(111) Semiconductor-on-metal growth: Formation of an Ag_2Ge surface alloy, Phys. Rev. B **62**, 16653 (2000).

[19] D. A. Muzychenko, A. I. Oreshkin, S. I. Oreshkin, S. S. Ustavschikov, A. V. Putilov, and A. Yu. Aladyshkin, The surface structures growth's features caused by Ge adsorption on the Au(111) surface, JETP Lett. **106**, 217 (2017).

[20] E. A. Martínez, J. D. Fuhr, O. Grizzi, E. A. Sánchez, and E. D. Cantero, Growth of germanene on Al(111) hindered by surface alloy formation, J. Phys. Chem. C **123**, 12910 (2019).

[21] R. Wu, I. K. Drozdov, S. Eltinge, P. Zahl, S. Ismail-Beigi, I. Božović, and A. Gozar, Large-area single-crystal sheets of borophene on Cu(111) surfaces, Nat. Nanotechnol. **14**, 44 (2019).

[22] C. Yue *et al.*, Formation of copper boride on Cu(111), Fundam. Res. **1**, 482 (2021).

[23] K. Zhang, D. Sciacca, A. Coati, R. Bernard, Y. Borensztein, P. Diener, B. Grandidier, I. Lefebvre, M. Derivaz, C. Pirri *et al.*, Resolving the structure of the striped Ge layer on Ag(111): Ag_2Ge surface alloy with alternate fcc and hcp domains, Phys. Rev. B **104**, 155403 (2021).

[24] K. Zhang *et al.*, Structure of germanene/Al(111): A two-layer surface alloy, J. Phys. Chem. C **125**, 24702 (2021).

[25] K. Zhang, R. Bernard, Y. Borensztein, H. Cruguel, and G. Prévot, Growth of germanium-silver surface alloys followed by *in situ* scanning tunneling microscopy: Absence of germanene formation, Phys. Rev. B **102**, 125418 (2020).

[26] J. Fang, P. Zhao, and G. Chen, Germanene growth on Al(111): A case study of interface effect, J. Phys. Chem. C **122**, 18669 (2018).

[27] W. Wang and R. I. G. Uhrberg, Coexistence of strongly buckled germanene phases on Al(111), Beilstein J. Nanotechnol. **8**, 1946 (2017).

[28] S. Endo, O. Kubo, N. Nakashima, S. Iwaguma, R. Yamamoto, Y. Kamakura, H. Tabata, and M. Katayama, Publisher's Note: "$\sqrt{3} \times \sqrt{3}$ germanene on Al(111) grown at nearly room temperature", Appl. Phys. Express **11**, 019201 (2018).

[29] D. A. Muzychenko, A. I. Oreshkin, A. D. Legen'ka, and C. Van Haesendonck, Atomic insights into single-layer and bilayer germanene on Al(111) surface, Mater. Today Phys. **14**, 100241 (2020).

[30] A. Dawiec, Y. Garreau, J. Bisou, S. Hustache, B. Kanoute, F. Picca, G. Renaud, and A. Coati, Real-time control of the beam attenuation with XPAD hybrid pixel detector, J. Instrum. **11**, P12018 (2016).

[31] S. Roobol, W. Onderwaater, J. Drnec, R. Felici, and J. Frenken, BINOCULARS: Data reduction and analysis software for two-dimensional detectors in surface x-ray diffraction, J. Appl. Crystallogr. **48**, 1324 (2015).

[32] G. Kresse, *Ab initio* molecular dynamics for liquid metals, J. Non-Cryst. Solids **192–193**, 222 (1995).

[33] G. Kresse and J. Hafner, *Ab initio* molecular-dynamics simulation of the liquid-metal–amorphous-semiconductor transition in germanium, Phys. Rev. B **49**, 14251 (1994).

[34] G. Kresse and J. Furthmüller, Efficiency of *ab-initio* total energy calculations for metals and semiconductors using a plane-wave basis set, Comput. Mater. Sci. **6**, 15 (1996).

[35] G. Kresse and J. Furthmüller, Efficient iterative schemes for *ab initio* total-energy calculations using a plane-wave basis set, Phys. Rev. B **54**, 11169 (1996).

[36] P. E. Blöchl, Projector augmented-wave method, Phys. Rev. B **50**, 17953 (1994).

[37] G. Kresse and D. Joubert, From ultrasoft pseudopotentials to the projector augmented-wave method, Phys. Rev. B **59**, 1758 (1999).

[38] J. P. Perdew, K. Burke, and M. Ernzerhof, Generalized Gradient Approximation Made Simple, Phys. Rev. Lett. **77**, 3865 (1996).

[39] J. P. Perdew, K. Burke, and M. Ernzerhof, Generalized Gradient Approximation Made Simple, Phys. Rev. Lett. **78**, 1396(E) (1997).

[40] P. V. C. Medeiros, S. Stafström, and J. Björk, Effects of extrinsic and intrinsic perturbations on the electronic structure of graphene: Retaining an effective primitive cell band structure by band unfolding, Phys. Rev. B **89**, 041407(R) (2014).

[41] P. V. C. Medeiros, S. S. Tsirkin, S. Stafström, and J. Björk, Unfolding spinor wave functions and expectation values of general operators: Introducing the unfolding-density operator, Phys. Rev. B **91**, 041116(R) (2015).

[42] J. Tersoff and D. R. Hamann, Theory and Application for the Scanning Tunneling Microscope, Phys. Rev. Lett. **50**, 1998 (1983).

[43] P. Haas, F. Tran, and P. Blaha, Calculation of the lattice constant of solids with semilocal functionals, Phys. Rev. B **79**, 085104 (2009).

[44] E. Golias, E. Xenogiannopoulou, D. Tsoutsou, P. Tsipas, S. A. Giamini, and A. Dimoulas, Surface electronic bands of submonolayer Ge on Ag(111), Phys. Rev. B **88**, 075403 (2013).

[45] W. Humphrey, A. Dalke, and K. Schulten, VMD: Visual molecular dynamics, J. Mol. Graph. **14**, 33 (1996).

[46] Theoretical and Computational Biophysics Group, VISUAL MOLECULAR DYNAMICS software, Beckman Institute for Advanced Science and Technology, University of Illinois, 2021 (www.ks.uiuc.edu/research/vmd/), (n.d.).

[47] D. A. Muzychenko, S. I. Oreshkin, V. I. Panov, C. Van Haesendonck, and A. I. Oreshkin, Single and multi domain buckled germanene phases on Al(111) surface, Nano Res. **12**, 2988 (2019).

[48] SciPy 1.0 contributors *et al.*, scipy 1.0: Fundamental algorithms for scientific computing in PYTHON, Nat. Methods **17**, 261 (2020).

[49] See Supplemental Material at http://link.aps.org/supplemental/10.1103/PhysRevB.106.045412 for theoretical STM image and band structure.